The International Journal of Engineering and Science (IJES)
|| Volume || 13 || Issue || 8 || Pages || PP 06-14 || 2024 ||
ISSN (e): 2319 – 1813 ISSN (p): 2319 – 1805

Design and mechanical behavior of scaffolding at the arch foot position of large-span cantilever casting concrete arch bridges

Yuexing W[1], Yi X[1*], Shuyao W[1], Zhengqing T[2], Mei W[3], Tao Y[4], Xingxin L[1], Linshu L[1]

[1] *College of Civil Engineering, Hunan City University, Yiyang, China*
[2] *CCCC First Highway Engineering Group Water Engineering Co., Ltd., Yiyang, China*
[3] *Hunan Art and Crafts Vocational College, Yiyang, China*
[4] *Hunan City University Test Centre Co., Ltd., Yiyang, China*
Corresponding Author: Yi X

----------ABSTRACT----------

Large-span reinforced concrete arch bridges are widely constructed in the mountainous regions of western China due to their high rigidity, low cost, and good durability. When constructing such arch bridges using the cantilever casting method, the abutment scaffolding, as an important temporary structure, plays a crucial role in ensuring the structural integrity and safety of the arch ring closure. This paper takes a 210-meter main span reinforced concrete arch bridge as an example. Based on the proposed special construction plan, the abutment scaffolding is preliminarily designed. A finite element model of the scaffolding is established using Midas/Civil software to analyze its mechanical behavior under various load conditions. The results are compared with the standard design values to verify the rationality of the temporary structure design. The research results indicate that the maximum axial tension-compression, bending, and shear stress of each component of the scaffolding is less their allowable stress respectively, and the maximum displacement is also less than the standard limit values, demonstrating that the scaffolding design is relatively reasonable. Observations of the actual bridge show that no buckling behavior occurred in any component of the scaffolding during the construction of the arch ring. The findings of this study are expected to provide valuable references for the design of scaffolding in the construction of similar arch bridges.

KEYWORDS;- *Reinforced concrete arch bridges; Cantilever casting method; Abutment scaffolding design; Midas/Civil software; Mechanical behavior*

Date of Submission: 03-08-2024 Date of acceptance: 14-08-2024

I. INTRODUCTION

With the rapid development of the economy and society, the demand for travel has increased dramatically, leading to the extensive construction of various types of bridges. Arch bridges are favored by domestic bridge engineers due to their high overall structural rigidity, reasonable force distribution, low construction cost, and good durability [1,2]. The reasonable design of bridge dimensions and structures, along with a matching construction plan, is crucial for the safe construction of arch bridges. Compared to steel arch bridges or steel tube concrete arch bridges, reinforced concrete arch bridges perform better and have fewer issues with structural corrosion during the operational period. The cantilever casting method, as a relatively common construction technique, can overcome the challenge of narrow construction sites where there is no prefabrication site when building reinforced concrete arch bridges, while also ensuring better integrity of the arch ring segments [3]. When using this construction method, scaffolding must first be erected at the abutment position of the arch bridge. The reasonable design of this scaffolding is essential to ensure the smooth construction of subsequent bridge segments [4].

Scholars around the world have conducted extensive research on the design and mechanical behavior analysis of bridge scaffolding. Zhang et al. [5] used the finite element method and material mechanics model to verify the stress and deformation of the large-span gate structure of the cast-in-place box girder bridge for urban viaduct. Shi [6] introduced several commonly used forms of scaffolds. Mehri et al. [7] studied the torsional bracing performance of a typical type of scaffoldings that are commonly used in bridge construction based on the experiment and numerical analysis. Yue [8] compared the construction technology and economic efficiency of the 56 m approach bridge by adopting two simple supported beam construction schemes between bailey beams and new combined truss girders. Sheng et al. [9] conducted the researches on the mechanical properties and deformation characteristics of the temporary support system of pile foundation underpinning. Diao et al. [10] used Midas/Civil to establish a finite element model of a mixed scaffolding system consisting of ringlock

scaffolding and beam-column scaffolding, verifying the feasibility of the cast-in-place scaffolding. Resende et al. [11] detailed the continuous monitoring of a full-scale Movable Scaffolding System during regular operation. Wang et al. [12] analyzed the primary deformation patterns of each component of the combined doorway through finite element simulation and theoretical derivation, utilizing the rigid body function of ANSYS. Jin et al. [13] developed a BIM-based tool and proposed to assist designers and builders in planning, designing, and generating concrete formwork design models for planning purposed. Liu [14] established a mathematical model for the relationship between the structural parameters and internal forces of the Renwanru river extra-large Bridge's scaffolding. He analyzed the internal force variation patterns of the main components of the scaffolding under different parameters and determined the optimal design scheme for the scaffolding's structural parameters. Wei et al. [15] elaborated on the design concepts and methods, as well as the key construction control points, for the tall steel tube beam-column cast-in-place scaffolding on steep slopes.

In summary, current research on scaffolding primarily focuses on tube beam-column cast-in-place scaffolding and bailey beams scaffolding, and the research methods include the establishment of mathematical models and finite element analysis. However, it rarely involves the design and mechanical behavior analysis of scaffolding for the arch foot segment of cantilever casting concrete arch bridges. Due to the largest inclination angle and often the heaviest weight of the No. 1 segment of the arch ring in an arch bridge, higher demands are placed on the load-bearing capacity of the scaffolding. A large-span cantilever cast-in-place concrete arch bridge is used as the engineering basis, and the scaffolding for the No. 1 segment of the arch ring is designed. A finite element model of the scaffolding is established using Midas/Civil software, and the structural strength, stiffness, and stability performance of the scaffolding are analyzed. These results are compared with the allowable values specified in the standards to verify the feasibility and rationality of the designed scaffolding.

II. BRIDGE OVERVIEW

The bridge route is designed as a full-width structure. The arrangement of bridge spans includes 2×30 m simply-supported and then continuous precast T-beams, a 210 m (net span) reinforced concrete box arch, and 3×30 m simply-supported and then continuous precast T-beams. The total length of the bridge is 391.4 m, with a center pile number of K44+775.000, a starting pile number of K44+593.800, and an ending pile number of K44+985.200. The main bridge's horizontal alignment is a straight line, and the vertical alignment consists of a convex curve with = ±0.5% and = 25445.380 m.

The main arch ring of the arch bridge adopts a catenary-shaped reinforced concrete box section, with a net span of = 210 m, a net rise of = 42 m, and a rise-to-span ratio of = 1/5. The arch axis coefficient is = 1.67. The arch box is a single-box single-chamber section with a half-width of 7.0 m and a box height of 3.5 m. The thickness of the top and bottom slabs of the cast-in-situ segment at the arch foot support varies from 80 cm to 40 cm, and the thickness of the web varies from 80 cm to 50 cm. For other segments of the arch ring, the top and bottom slabs are 40 cm thick, and the web thickness is 50 cm. Segment No. 1 at the arch foot is constructed using cast-in-situ scaffolding, segments No. 2 to No. 14 are constructed using cantilevered form travelers, and the closure segment at the crown is constructed using a steel skeleton encased in concrete. The arch ring construction buckling cables are installed at the position of the transverse diaphragms at the ends of each segment, with fixed-end round P anchors used for anchoring. After the main arch ring construction is completed, the buckling cables are cut, and the cable holes are grouted and filled [16,17]. The elevation layout of the arch bridge and the cross-sectional layout are shown in Figure 1 and Figure 2, respectively.

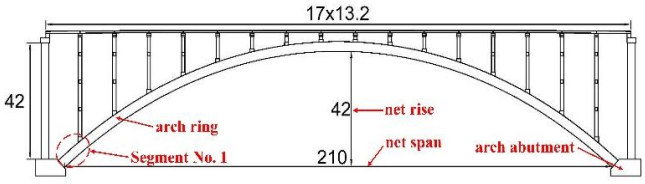

Figure 1 The elevation layout of the arch bridge (units: m)

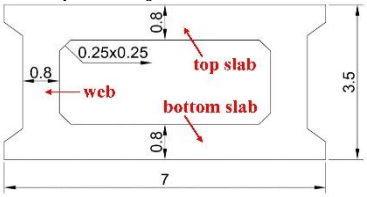

Figure 2 The cross-sectional layout (units: m)

III. SCAFFOLDING OVERVIEW

The weight of the No. 1 segment at arch foot position is relatively heavy (=362.0 t), and the arch segment is an inclined structure. The load transmitted to the scaffolding through the bottom formwork includes not only vertical loads but also significant horizontal loads. For the concrete pouring of the No. 1 segment at arch foot position, a steel tube scaffolding support system is utilized. To overcome the horizontal loads on the scaffolding, steel sections are embedded in the arch abutment and welded to the longitudinal horizontal rods.

Since the location of the arch abutment is on bedrock, the foundation treatment for the entire steel tube scaffolding is relatively easy. Spiral welded tubes with dimensions of 630×12 mm are used to fabricate the scaffolding columns on-site. The scaffolding steel tubes are arranged in three longitudinal rows (in the direction of the bridge progression), with each row consisting of two tubes, totaling six steel tubes. At the top of each row,

two I40b steel sections are placed, connecting the two transverse steel tubes together. Five sets of two I40b steel sections are longitudinally placed on top of the transverse distribution beams, forming a three-span continuous beam. Except for the side near the arch abutment, which is connected to the embedded steel sections with steel plates as connection plates, the other connections are made by directly welding the I40b steel sections to wedge-shaped blocks. The bottom formwork distribution beams (I20b) are then placed on the I40b steel sections at 60 cm intervals, and the bottom formwork for the box arch is installed on top of these distribution beams. To accommodate the curvature changes of the arch ring, adjustment blocks are set between the transverse and longitudinal steel sections to ensure the proper alignment of the bottom formwork. Due to the steep incline of the arch foot segment, 1.5 m long I40b steel sections are embedded in the arch abutment (1 m embedded in concrete and 0.5 m extending out of the concrete) to resist the horizontal thrust during the concrete pouring of the arch foot segment and to maintain the stability of the scaffolding. The elevation layout of the scaffolding at the arch foot position of the arch bridge is shown in Figure 3, and on-site construction image of the scaffolding is shown in Figure 3.

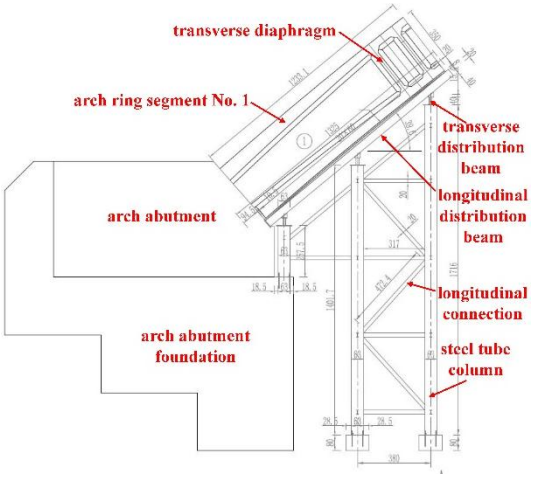

Figure 3 The elevation layout of the scaffolding (units: cm)

Figure 4 On-site construction image of the scaffolding

IV. LOAD ANALYSIS AND FINITE ELEMENT MODEL ESTABLISHMENT

When conducting the scaffolding stress analysis, the following loads typically need to be considered: the self-weight of the formwork, the concrete load, the load from construction personnel, the load from construction materials, the load from machinery and equipment during transportation or storage, crowd load, and the load from concrete vibration. Ribbed steel formwork is used, with a weight of 150kg per square meter being considered. The cast-in-situ concrete unit weight is considered to be . According to Figure 2, the formwork self-weight at the web position is , and the formwork self-weight at the top/bottom slab position is . The concrete load at the web position is , and the concrete load at the top/bottom slab position is . The load from construction personnel, the load from construction materials, the load from machinery and equipment during transportation or storage is considered at . The load from concrete vibration is considered at . It is particularly important to note that when verifying the strength of the scaffolding structure, all the aforementioned types of loads need to be considered. While verifying the stiffness of the scaffolding structure, only the dead loads need to be considered, which include the self-weight of the formwork and the concrete load.

Based on the special construction plan for the scaffolding and the relevant information from the bridge design drawings, a finite element model is established using Midas/Civil software. Except for the bottom formwork, which is simulated using plate elements, all other components of the scaffolding are simulated using beam elements. All degrees of freedom at the bottom of the steel tube columns are constrained, and the same constraint conditions are applied to the longitudinal distribution beam at the arch abutment end. The aforementioned loads are applied to the bottom formwork elements in the form of uniformly distributed surface loads. The specific operations for finite element modeling can be referred to in the literature [18]. The finite element model of the cast-in-situ scaffolding for the No. 1 segment of the arch ring and the load diagram is shown in Figure 5.

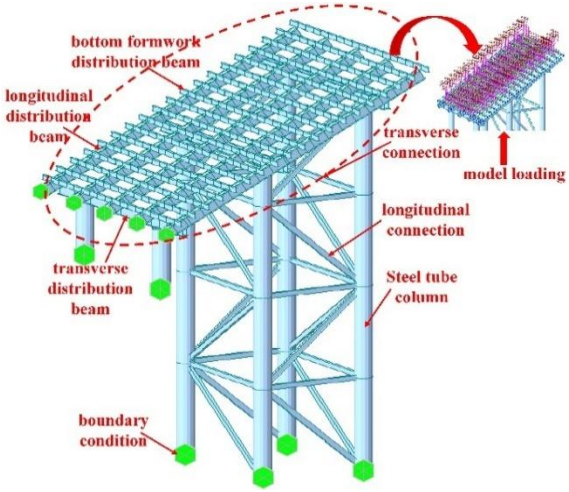

Figure 5 The finite element model of the cast-in-situ scaffolding

V. Analysis of the Results from the Scaffolding Finite Element Model

(1) Scaffolding strength analysis

1) Verification of the bottom formwork distribution beams

The bottom formwork distribution beams are primarily subjected to bending and shear forces. According to their stress characteristics, analysis and calculation of bending and shear stress conditions are conducted. The calculation results of bending and shear stress of the bottom formwork distribution beams are shown in Figure6 and Figure7, respectively.

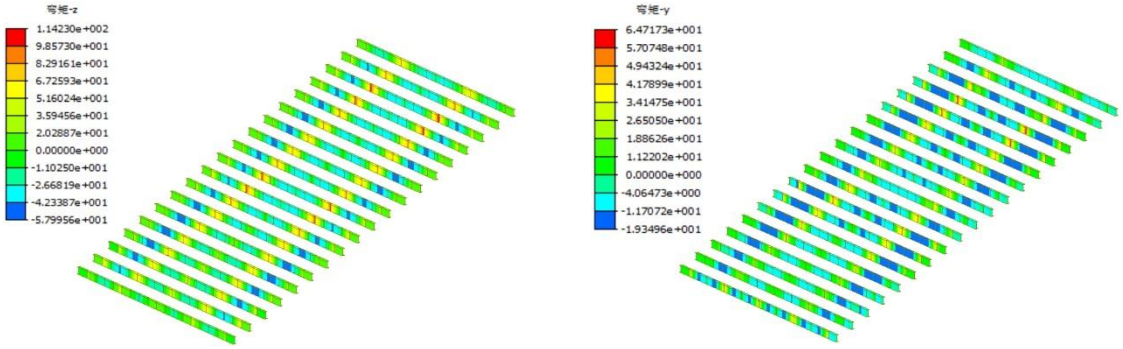

(a) Z-direction bending stress (b) Y-direction bending stress

Figure 6 The calculation results of bending stress of the bottom formwork distribution beams (units: MPa)

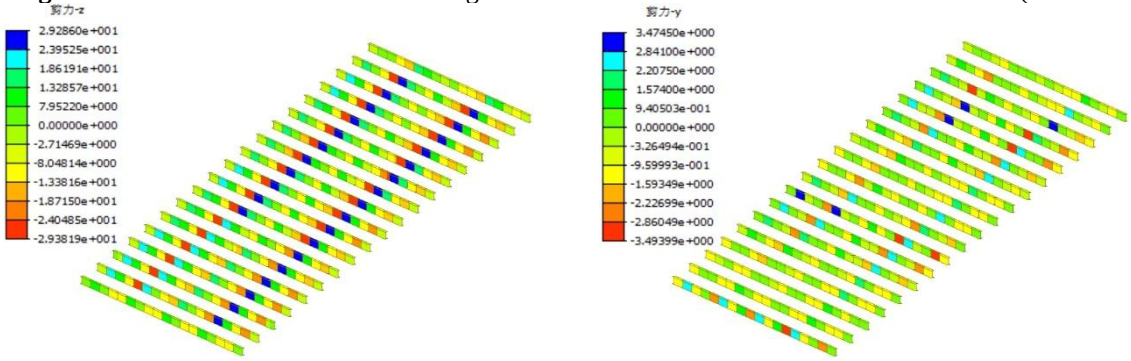

(a) Z-direction shear stress (b) Y-direction shear stress

Figure 7 The calculation results of shear stress of the bottom formwork distribution beams (units: MPa)

From Figure 6, it can be observed that the maximum Z-direction and Y-direction bending stress experienced by the bottom formwork distribution beams which are made of Q235 steel is 114.2 MPa and 64.7MPa respectively. The maximum allowable tensile stress for Q235 steel is 205 MPa, with a safety factor of 1.8 and 3.2 respectively, indicating that the bending strength requirements are satisfied. According to Figure 7, it can be seen that the maximum Z-direction and Y-direction shear stress experienced by the bottom formwork distribution beams is 29.4MPa and 3.5MPa respectively. The maximum allowable shear stress is 120MPa, with a safety factor of 4.1 and 34.3 respectively, indicating that the shear strength requirements are satisfied.

2) Verification of the longitudinal distribution beams

The longitudinal main beams are arranged along the longitudinal direction of the bridge with a tilt, primarily subjected to axial stress, bending, and shear. According to their stress characteristics, analysis of axial tension-compression, bending, and shear stress is conducted. The calculation results of bending, shear and axial tension-compression stress of the longitudinal distribution beams are shown in Figure8, Figure9 and Figure10, respectively.

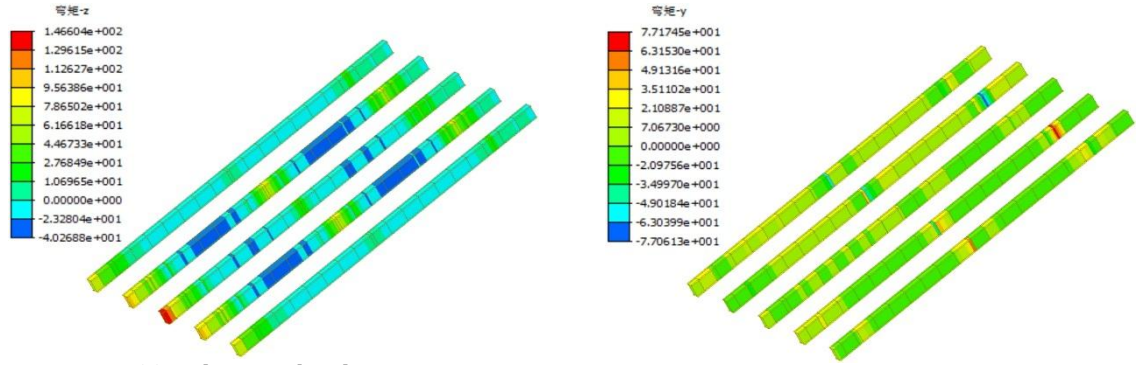

(a) Z-direction bending stress (b) Y-direction bending stress

Figure 8 The calculation results of bending stress of the longitudinal distribution beams (units: MPa)

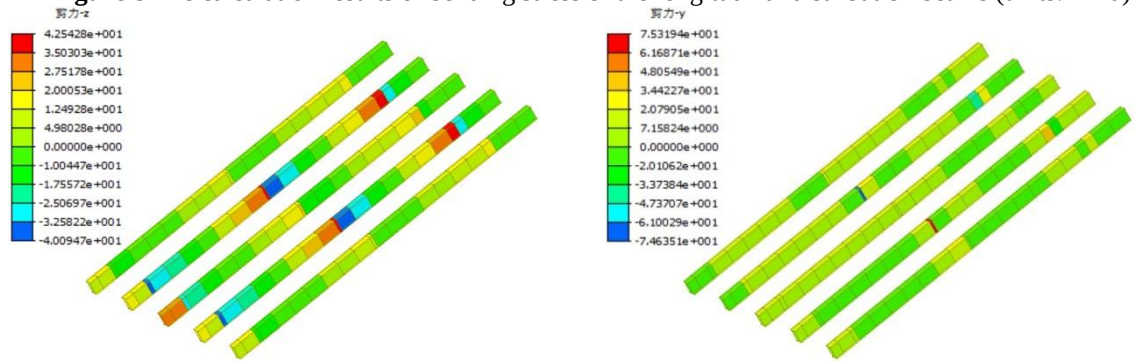

(a) Z-direction shear stress (b) Y-direction shear stress

Figure 9 The calculation results of shear stress of the longitudinal distribution beams (units: MPa)

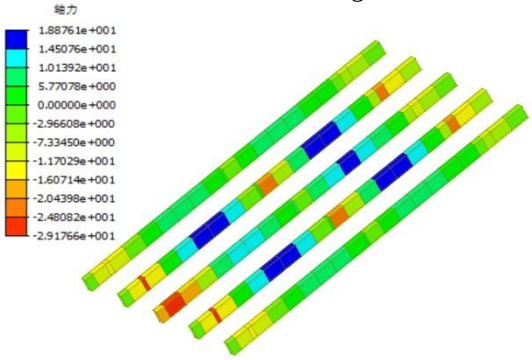

Figure 10 The calculation results of axial stress of the longitudinal distribution beams (units: MPa)

According to Figure 8, the maximum Z-direction and Y-direction bending stresses borne by the longitudinal distribution beams are 146.6 MPa and 77.2 MPa respectively. These values are less than the maximum allowable tensile stress of 205 MPa for the component. The safety factors are 1.4 and 2.7 respectively,

indicating that the bending strength requirements are met by the specifications. According to Figure 9, it can be seen that the maximum Z-direction and Y-direction shear stresses experienced by the longitudinal distribution beams are 42.5 MPa and 75.3 MPa respectively. These values are less than the maximum allowable shear stress of 120 MPa for the component. The safety factors are 2.8 and 1.6 respectively, indicating that the shear strength requirements are met by the specifications.

According to Figure 10, it can be observed that the maximum axial tensile stress experienced by the longitudinal distribution beams is 18.9 MPa, which is less than the maximum allowable tensile stress of 205 MPa for the component. The safety factor is 10.8, indicating that the tensile strength requirements are satisfactorily met. The maximum axial compression stress is -29.2MPa. According to the reference [19], the main beam is classified as a class b component, with a bracing reduction factor of 0.78. After considering the reduction factor for the compression member, the maximum allowable axial stress of the component is 159.9 MPa. The safety factor is 5.5, indicating that the compression strength requirements are satisfactorily met too.

3) Verification of the transverse distribution beams

The steel tube distribution beam is horizontally arranged along the transverse directions of the bridge, used to support the longitudinal main beam. It mainly bears bending and shear forces. Based on its force characteristics, a bending and shear force analysis is conducted. The calculation results of bending and shear stress of the transverse distribution beams are shown in Figure11 and Figure12, respectively.

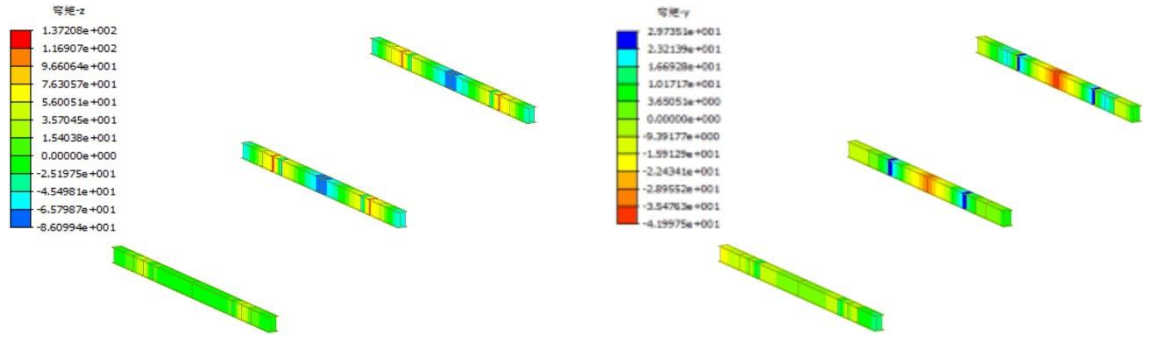

(a) Z-direction bending stress (b) Y-direction bending stress

Figure 11 The calculation results of bending stress of the transverse distribution beams (units: MPa)

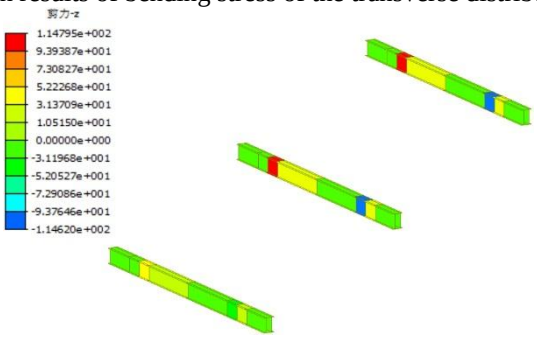

Figure 12 The calculation results of shear stress of the transverse distribution beams (units: MPa)

According to Figure 11, the maximum Z-direction and Y-direction bending stresses borne by the transverse distribution beams are 137.2 MPa and 42.0 MPa respectively. These values are less than the maximum allowable tensile stress of 205 MPa for the component. The safety factors are 1.5 and 4.9 respectively, indicating that the bending strength requirements are met by the specifications. According to Figure 12, it can be seen that the maximum Z-direction shear stresses experienced by the transverse distribution beams are 114.8 MPa. Which is less than the maximum allowable shear stress of 120 MPa for the component. The safety factors are 1.05, indicating that the shear strength requirements are met by the specifications.

4) Verification of the steel tube columns

The ϕ 630×12 mm steel tube piles are used as the intermediate piers, with transverse and longitudinal connections set at a maximum interval of 3.8 m. Therefore, the height of the steel tube piles is calculated as 3.8 m. The axial stress of the steel tube columns is shown in Figure13.

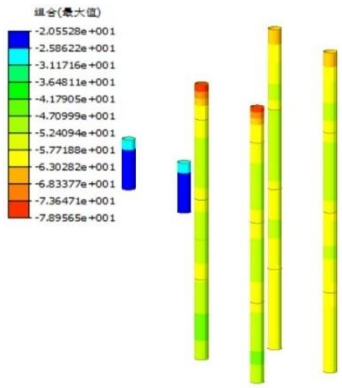

Figure 13 The calculation results of axial stress of the steel tube columns (units: MPa)

From Figure 13, it can be seen that the maximum combined stress on the steel tube column is 79.0 MPa. With a maximum free length of 3.8m for the member, considering the member as a type b component, the slenderness ratio is 34.0, and the reduction factor for the compression member is 0.922. Therefore, the maximum allowable compressive stress of the component is 189.0 MPa, indicating that the steel tube piles meet the strength and stability requirements for compression members.

5) Verification of reactions at each support point

The support reaction force results of the scaffolding are shown in Figure14.

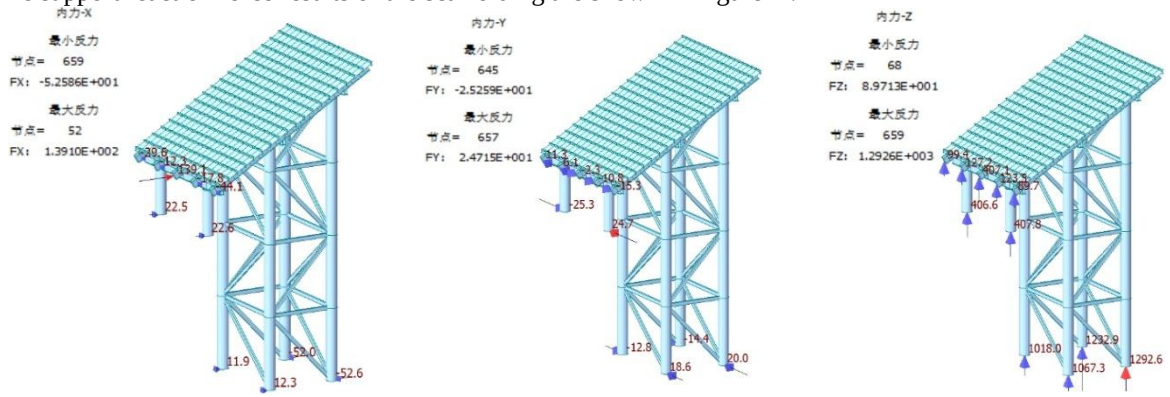

(a) X-direction support reaction (b) Y-direction support reaction (c) Z-direction support reaction

Figure 14 The support reaction force results of the scaffolding (units: kN)

From Figure14, it can be seen that the maximum X-direction, Y-direction and Z-direction support reaction force is 139.1 kN, 24.7 kN and 1292.6 kN respectively. The maximum Z-direction reaction force acts directly on the foundation, and it is necessary to verify the bearing capacity of the foundation. The auxiliary pier foundation is constructed using C25 concrete, with foundation dimensions of 1.2 m × 1.2 m × 0.8 m. The maximum load on the foundation is 1292.6 kN, and the self-weight of the foundation is 26.2 kN. Therefore, the required bearing capacity of the foundation base is 915.8 kPa. For safety reasons, foundation bearing capacity is required to be no less than 1.5 MPa in the support design drawings.

(2) Scaffolding stiffness analysis

The overall deformation of the scaffolding is shown in Figure15. The deformation of longitudinal and transverse distribution beams of the scaffolding is shown in Figure16.

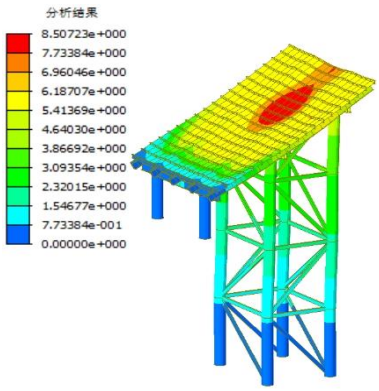

Figure 15 The overall deformation of the scaffolding (units: mm)

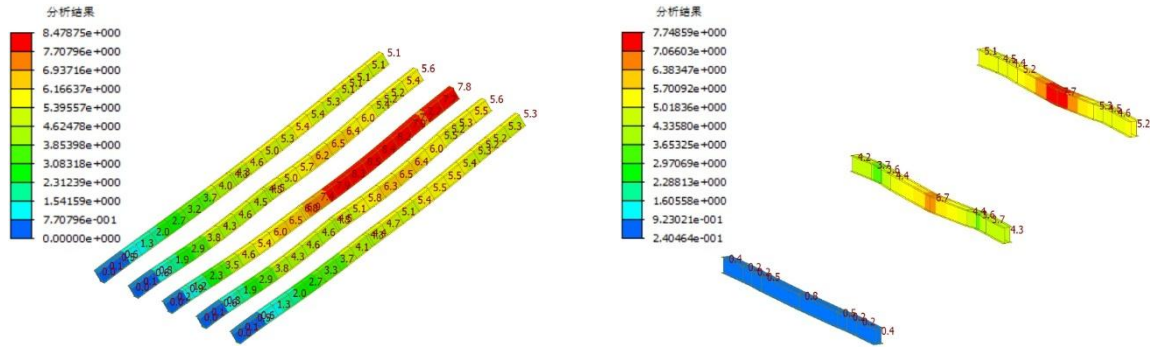

(a) The deformation of longitudinal distribution beams (b) The deformation of transverse distribution beams

Figure 16 The deformation of the scaffolding component (units: mm)

From Figure15, it can be seen that the maximum overall deformation of the scaffolding is at the bottom slab of the box girder near the mid-span position, with a maximum deformation value of 8.5 mm. From Figure 16, the maximum elastic deflection of the longitudinal distribution beam is 8.5 mm. According to the reference [20], the elastic deflection of the loaded members of the scaffolding should be 1/400 of the calculated span of the corresponding structure. Based on this regulation, the maximum elastic deflection is calculated to be 9.5 mm. Therefore, the calculated maximum deflection is less than the allowable deflection, and the maximum deflection meets the stiffness deformation requirements. the maximum elastic deflection of the transverse distribution beams is 7.7 mm, which is less than the corresponding allowable deflection 12.5 mm, indicating the structural stiffness meets the requirements of the specifications.

VI. CONCLUSION

Taking a large-span cantilever cast-in-situ concrete arch bridge as the engineering basis, and the scaffolding for the No. 1 segment of the arch ring is designed. A finite element model of the scaffolding is established using Midas/Civil software, and the structural strength, stiffness, and stability performance of the scaffolding under different conditions are analyzed. The main conclusions are listed as follows:

1) The bending and shear resistance verification of the bottom formwork distribution beam meets the specification requirements. The safety factors for axial tension, bending, and shear resistance of the longitudinal and transverse distribution beams meet the specification requirements, and the deformation under load meets the specification requirements too. The steel tube columns meet the stability requirements for compression members. Observations of the actual bridge show that no buckling behavior occurred in any component of the scaffolding during the construction, which proves that the design of this scaffolding is reasonable.

2) During construction, attention should be paid to the stability of the steel tube piles themselves, and the connection between the pipes should be strengthened both horizontally and longitudinally, as well as the connection between the members and the arch abutment. The longitudinal distribution beams embedded in the arch abutment bears a large horizontal load (mainly pressure). During construction, steel mesh should be added at the location where the longitudinal distribution beams is embedded to increase the local bearing capacity.

3) The shortcomings of this paper lie in the simplification of the concrete vibration load as a static load when calculating its impact on the scaffold stress, failing to precisely consider its impact effect on the scaffolding. However, the form of the scaffolding, its design concept, and the method of validating structural bearing capacity through finite element modeling presented in this paper can provide valuable references for future similar arch bridge projects.

FUNDING

The author(s) declare that financial support was received for the research, authorship, and/or publication of this article. This research was funded by Undergraduate Innovation and Entrepreneurship Training Plan Program of Hunan Province, China (grant number S202311527025), the Natural Science Foundation of Hunan Province, China (grant numbers 2024JJ7077 and 2024JJ7170) and the Research Foundation of Education Bureau of Hunan Province, China (grant numbers 23B0732, 22A0561 and 23A0559).

REFERENCE

[1]. Deaver RW. Bridge Widening Study, Research Report: No. 7604. Georgia Department of Transportation, Georgia, USA, 1982.
[2]. Liu Z W, Zhou S X, Zou K R, et al. A numerical analysis of buckle cable force of concrete arch bridge based on stress balance method[J]. Scientific Reports, 2022, 12: 12451.
[3]. Sun J P, Li J B, Jiang Y B, et al. Key construction technology and monitoring of long-span steel box tied arch bridge[J]. International Journal of Steel Structures, 2023, 23(1): 191-207.
[4]. Liu Z W, Zhou J T, Wu Y X, et al. Linear control method for arch ring of oblique-stayed buckle cantilever pouring reinforced concrete arch bridge[J]. Advances in Civil Engineering, 2021, 6633717.
[5]. Li Y M, Bai X H, W Q F. Design characteristics and cast-in-place construction technology of variable width continuous box girders on mountainous roads using scaffolding method[J] Journal of China & Foreign Highway, 2022, 42(6): 146-151 (in Chinese).
[6]. Zhang Y, Li J Q, Luo Z J, et al. Design and construction of long span gateway opening for cast-in-situ box girder of urban viaduct[J]. Bridge Construction, 2012, 42(S1): 144-147 (in Chinese).
[7]. Shi B Q. The construction technology of T-type rigid frame bridge No. 0 pouring section[J]. Applied Mechanics and Materials, 2014, 587-589: 1713-1717 (in Chinese).
[8]. Mehri, H, Crocetti, R. Scaffolding bracing of composite bridges during construction[J]. Journal of Bridge Engineering, 2016, 21(3): 04015060.
[9]. Yue X G. construction scheme comparison and selection between new combined truss girder and bailey beam[J]. Railway Engineering, 2018, 58(5): 34-38 (in Chinese).
[10]. Sheng H, Li H W, Gu X Y, et al. Researches on the mechanical properties and deformation characteristics of the temporary support system of pile foundation underpinning[J]. Building Structure, 2021, 51(S2): 1545-1550 (in Chinese).
[11]. Diao Z S, Liu B. Design and key construction technology of long-span T-frame combined bracket[J]. Urban Roads Bridges & Flood Control, 2023, (5): 143-147 (in Chinese).
[12]. Resende, A, Pereira, S, Magalhães, F, et al. Continuous monitoring of a large movable scaffolding under operation[J]. Automation in Construction, 2023, 156: 105084.
[13]. Wang W M, Yang Z, Guo C, et al. Deformation analysis and optimization of steel-tube-columns combined-with-bailey-beams doorway support[J] Buildings, 2023, 13: 2541.
[14]. Jin, Z, Gambatese, J. BIM-based timber formwork design and modeling[J]. Practice Periodical on Structural Design and Construction, 2023, 28(1): 04022057.
[15]. Liu Z H. A study on the optimization design of bridge construction scaffolding driven by parametric analysis[J]. Highway, 2024, 5: 247-250 (in Chinese).
[16]. Wei Z H, Liu Y, Nan W Z, et al. Design and construction technology of high and large cast-in-place bridge scaffold on steep slopes[J]. Highway, 2024, (2): 52-57 (in Chinese).
[17]. Li X J, ZHOU J T, Wu Y X, et al. Structural analysis and improvement for a new form traveler in long-span cantilever-casting arch bridge[J]. Advances in Civil Engineering, 2021, 13(4): 1-13.
[18]. Sun Y, Xu Y, Guo J P, et al. Constructional safety-based cost optimization for the buckling-anchorage system of cantilever casting concrete arch bridge[J]. Journal of Bridge Engineering, 2022, 27(5): 04022022.
[19]. Ge J Y. Bridge engineering software Midas Civil user guide[M]. Beijing: China Communications Press, 2013 (in Chinese).
[20]. GB 50017-2014. Code for design of steel structure[S]. Ministry of Construction of the People's Republic of China (in Chinese).
[21]. JTG/T 3650-2020. Technical Specifications for construction of highway bridges and culverts[S]. Ministry of Transport of the People's Republic of China (in Chinese).